Journal of Nuclear Materials 509 (2018) 465–477

Contents lists available at ScienceDirect

Journal of Nuclear Materials

journal homepage: www.elsevier.com/locate/jnucmat

Phase quantification in UAl_x-Al dispersion targets for Mo-99 production

G.L.C.R. Conturbia [a], M. Durazzo [a, *], E.F. Urano de Carvalho [a], H.G. Riella [a, b]

[a] Nuclear and Energy Research Institute, IPEN/CNEN-SP, São Paulo, Brazil
[b] Chemical Engineering Department, Santa Catarina Federal University, Florianópolis, Brazil

HIGHLIGHTS

- Image analysis and X-ray diffraction methods for phase quantification of UAl_x phases.
- Mapping UAl_x phase composition during target fabrication.
- Following UAl_2 transformation during rolling UAl_x-Al dispersion targets.

GRAPHICAL ABSTRACT

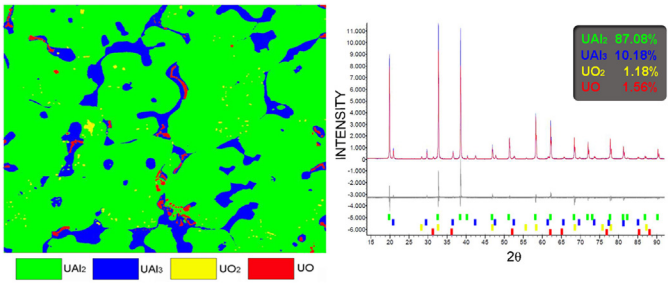

ARTICLE INFO

Article history:
Received 4 April 2018
Received in revised form
3 July 2018
Accepted 13 July 2018
Available online 18 July 2018

Keywords:
UAl_x-Al
Irradiation targets
Molybdenum-99
Phase quantification
Image analysis
Rietveld method

ABSTRACT

Uranium aluminide (UAl_x) is a mixture of three distinct intermetallic compounds comprised of UAl_2, UAl_3 and UAl_4, where the "x" is used to denote a mixture of those phases. Usually UAl_x is formed during the target fabrication process by means of a solid state reaction between the uranium aluminide and aluminum. Quantitative techniques such as image analysis and X-ray diffraction using the Rietveld method were compared for their applicability in the determination of the UAl_2, UAl_3 and UAl_4 concentrations, both in the UAl_2 primary ingot and in the UAl_x-Al dispersion. The UAl_x composition was quantified in all stages of the target manufacturing. The image analysis method was shown to be useful for UAl_x phase quantification in the primary UAl_2 ingot, but was not applicable in the case of UAl_x-Al dispersions. The X-ray diffraction method allowed the quantification of the existing UAl_x phases in both the primary ingot and UAl_x-Al dispersions. Possible sources of error are discussed. The method of quantification based on X-ray diffraction was shown to be appropriate to monitor the evolution of UAl_x phases during the manufacturing process.

1. Introduction

Every year the world demands more than 30 million medical imaging procedures that use the technetium-99 m radioisotope (Tc^{99m}), which correspond to approximately 80% of all nuclear medicine diagnoses [1]. This radiopharmaceutical product stems from the radioactive decay of molybdenum-99 (Mo^{99}), which is commercially produced in research reactors by irradiating targets that contain uranium-235. However, continuous supply of Mo^{99} has decreased over the last decade, mainly due to shutdowns that have occurred in the main research reactors that produce radioisotopes [1]. To deal with this scenario, Brazil has decided to build a

* Corresponding author. Av. Prof. Lineu Prestes, 2242, Cidade Universitária, CEP 05508-000, São Paulo, SP, Brazil.
E-mail address: mdurazzo@ipen.br (M. Durazzo).

https://doi.org/10.1016/j.jnucmat.2018.07.029
0022-3115/

multipurpose reactor which among other functions will irradiate uranium targets to produce enough Mo-99 to meet domestic demand [2,3].

There are currently two technologies available to produce uranium targets. One is based on a uranium-aluminum compound dispersed in an aluminum matrix [4–9] and the other one is based on metallic uranium thin foils [10–14]. The dispersed targets are the most used worldwide for commercial production of molybdenum-99 b y nuclear fission. The targets use low enriched uranium (LEU) and are fabricated according to traditional technology based on the picture-frame technique [15–17], which is adopted for commercial production of fuel elements for nuclear research reactors. Because of the experience acquired over the years in the manufacturing of dispersion fuel elements, it was decided to implement this technology to fabricate UAl_x-Al dispersion targets for future molybdenum-99 production in Brazil.

The binary system, uranium and aluminum, forms a phase diagram which shows the existence of intermetallic compounds consisting of three phases, namely UAl_2, UAl_3, and UAl_4. The mixture of these phases is known in the literature as UAl_x [18]. It has been reported that UAl_3 and UAl_4 are more easily dissolved in alkaline solutions than UAl_2, which ultimately defines the radiochemical processing yield after the irradiation [19]. Therefore it is desirable for UAl_3 and UAl_4 phases to be present in the final target as they show good basic dissolution behavior during the subsequent radiochemical processing.

UAl_2 has been used as starting material for the fabrication of the irradiation targets [4–9]. The use of UAl_2 instead of other aluminides offers advantages in terms of its synthesis since the UAl_2 has a congruent melting point and as a result it can be synthesized in a single step, requiring no post-synthesis annealing. UAl_3 and UAl_4 have incongruent melting points and thus are formed through peritetic reactions, requiring long thermal treatments to complete synthesis [18,20]. Moreover, UAl_2 has higher U-content (81.52 wt% U) and density (8.14 g/cm^3) than the other uranium aluminides and therefore it maximizes the uranium-235 content in the target.

UAl_x-Al dispersion targets are fabricated by hot-rolling according to the traditional picture-frame technique [15–17] as small aluminum plates containing a UAl_x-Al dispersion meat. During fabrication UAl_2 reacts with aluminum to form UAl_3 and UAl_4 during the thermal-mechanical and annealing processes [5,9].

An important requirement for the target is the limitation of the UAl_2 content in the finished target, which should preferably to be zero. As already mentioned, this limitation is due to the fact that the uranium aluminides have different chemical properties with respect to their dissolutions in basic medium for the extraction of molybdenum-99 after irradiation. For example, Cols et al. [19]. Reported that UAl_3 and UAl_4 dissolve more easily in alkaline medium than UAl_2, and this defines the yield of radiochemical processing for Mo-99 extraction.

On the one hand, UAl_2 is used as starting material to fabricate the target. On the other hand, it must be totally consumed at the end of thermal mechanical processing. Therefore the UAl_2 assay must be quantified before and after thermal processing to ensure that all UAl_2 has been consumed. Thus, characterizing the phase composition in the starting material and UAl_x dispersions is important to assess the UAl_2 transformation during target fabrication, so that a thermo-mechanical treatment can be developed to ensure that all UAl_2 is consumed during manufacturing and will not be present in the final target.

This work aims to investigate methods to quantify the phases present in UAl_2 ingots and also in UAl_x-Al dispersion targets. Image analysis and X-ray diffraction were assessed as two possible methods.

2. Experimental procedures

The uranium dialuminide (UAl_2) was prepared by induction melting method and the uranium and aluminum were weighed-in stoichiometrically (81.5 wt% U) [20]. Then, the metals were charged into a zirconium crucible and melted using a 15 kW induction furnace. Prior the melting, the furnace was purged with argon after vacuum of 2.6×10^{-3} mbar. The UAl_x ingot was ground in a mortar under argon atmosphere. The grinding product was sieved in 8-in. (204 mm)-diameter stainless steel sieves. Three particles sizes were separated: +170 mesh (>88 μm), −170 + 325 mesh (<88 μm and >44 μm), and −325 mesh (<44 μm). The fuel powders used in the fabrication of targets were 80%−170 + 325 mesh and 20% −325 mesh. The density of the UAl_2 powder was determined to be 8.13 ± 0.01 g/cm^3 (triplicate) by helium pycnometry. The uranium content was determined to be 80.74 ± 0.02 wt% (triplicate) by chemical analysis [21,22].

Mixtures of aluminum and UAl_2 powders corresponding to 50 and 45% in volume respectively were homogenized for 1 h in a blender (Turbula T2F) and then compacted under pressure of 490 MPa to produce briquettes with porosity around 5 vol%. After compacting, the briquettes were degassed at 250 °C for 3 h under vacuum (5.10^{-3} Pa). Table 1 presents the typical characteristics of briquettes.

The briquettes were assembled into aluminum picture frames (4.20 mm thick) which were clad with two aluminum plates (2.86 mm tick). The assemblies were TIG (Tungsten Inert Gas) welded together and then rolled to form the targets, according to the picture-frame technique [15–17]. The assemblies were hot-rolled in six rolling passes. The final thickness for the target was reached through the cold-rolling pass. Fig. 1 illustrates the main

Table 1
Main typical characteristics of briquettes.

	Dimensions (mm)	22.16 × 22.15 X 4.20 (thickness) (with rounded corners/R = 3.0 mm)
Briquette	Mass (g)	9.67
	Volume (cm^3)	1.94
	Mass (g)	2.65
Aluminum	Mass fraction (%)	27.4
	Volume (cm^3)	0.98
	Volume fraction (%)	50.5
	Mass (g)	7.02
UAl_2	Mass fraction (%)	72.6
	Volume (cm^3)	0.86
	Volume fraction (%)	44.3
Pores	Volume (cm^3)	0.10
	Volume fraction (%)	5.2

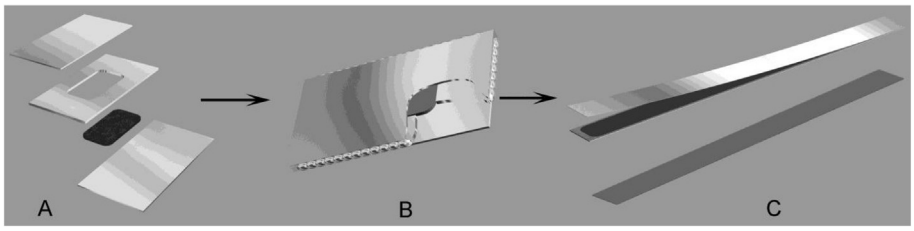

Fig. 1. Fabrication of UAl_x-Al dispersion targets.
A-picture-frame assembling, B – welding, C – after rolling.

steps to produce the UAl_x-Al dispersion target.

In order to define the rolling temperature at which UAl_2 were consumed fastest the thermomechanical process was carried out in various temperatures. After rolling, the targets were heat treated during cumulative time to follow quantitatively the UAl_x phase evolution profile over time. Table 2 shows a typical rolling scheme adopted to manufacture UAl_x-Al dispersion targets. Before the first rolling pass, the assembly was held at the rolling temperature for 1 h. The assembly was reheated for 15 min between passes. After the last pass, the assembly is again held at the rolling temperature for 1 h. Therefore, during the hot-rolling, the total heating time was 3 h and 15 min (3.25 h).

The phase composition was quantified by studying the microstructures of the ingot and UAl_x-Al dispersion through scanning electron microscopy (backscattered electron image) and EDS (energy-dispersive X-ray spectroscopy). A FEI Quanta 650 FEG scanning electron microscope was used with an Oxford XMAX spectroscope. The quantitative image analysis was carried out by mean of Omnimet® Enterprise Buehler® software [23,24].

X-ray diffraction data were also collected from samples of UAl_2 powder and UAl_x-Al compact utilizing a Bruker diffractometer, operating with Cu-Kα radiation at 40 kV and 30 mA, with a scan of 0.02° and for 8 s counts per step. The reference information was obtained from ICSD files 58195, 58196, 24012, 647597, 24233 and 43423, for UAl_2, UAl_3, UAl_4, UO_2, UO, and aluminum respectively [25–30]. The crystalline phases were quantified using the Rietveld method [31,32] with TOPAS V 4.2 for data refinement.

All the uncertainties presented refer to ±1 standard deviation (1 sigma).

3. Results and discussion

3.1. Phase quantification in the UAl_2 primary ingot

A scanning electron micrograph of the primary UAl_2 ingot is shown in Fig. 2. Because of the atomic number contrast obtained from backscattered electrons, which is sensitive to the composition, it was possible to observe four shades of gray indicating the existence of four phases. The microstructure showed the formation of UAl_2 (in lighter gray) as the predominant phase and UAl_3 (in dark gray) as the minority phase, which was formed during the solidification of residual liquid phase at UAl_2 grain boundaries. Inclusions with lighter grays than UAl_2 can be also seen in the image. These inclusions come from denser phases than UAl_2, since they have lighter gray tones in the backscattered electron image. One of these phases is almost white (the densest phase) and is mainly embedded in the UAl_3 phase. The other, slightly less dense than UAl_2 (light gray) is embedded in the UAl_2 matrix.

In order to investigate these phase's compositions, semi-quantitative EDS analysis showed that the darkest phase is composed of uranium and aluminum in the proportion of 75.5 wt% and 24.5 wt%, respectively, close to the composition of UAl_3 (74.6 wt % uranium, 25.4 wt% aluminum). The matrix phase, which appears in a lighter gray shade, had a composition of 83.2 wt% uranium and 16.8 wt% aluminum, close to the UAl_2 composition (81.5 wt% uranium and 18.5 wt% aluminum). The inclusions showed the presence of uranium and oxygen in their compositions. The inclusion with a slightly lighter shade of gray than UAl_2 had a composition of 88.4 wt% uranium and 11.6 wt% oxygen, a composition close to that of UO_2 (88.2 wt% uranium and 11.8 wt% oxygen). The almost whitish inclusion presented a composition of 93.1 wt% uranium and 6.9 wt% oxygen, a composition close to UO (93.7 wt% uranium and 6.3 wt% oxygen).

The ingot was crushed and ground into powder and the presence of these phases was confirmed by X-Ray diffraction. The oxide inclusions are present in minor concentrations, as can be seen in the diffractogram shown in Fig. 3. The major constituent is the UAl_2

Table 2
Typical rolling schedule for manufacturing UAl_x-Al dispersion targets.

	Pass Number	Reduction (%)	Gage (mm)	
Start	0		9.92	heating for 1 h
Hot	1	29	7.04	15 min reheating
	2	26	5.20	15 min reheating
	3	25	3.90	15 min reheating
	4	28	2.81	15 min reheating
	5	21	2.21	15 min reheating
	6	24	1.69	heating for 1 h
Cold	7	8	1.55	

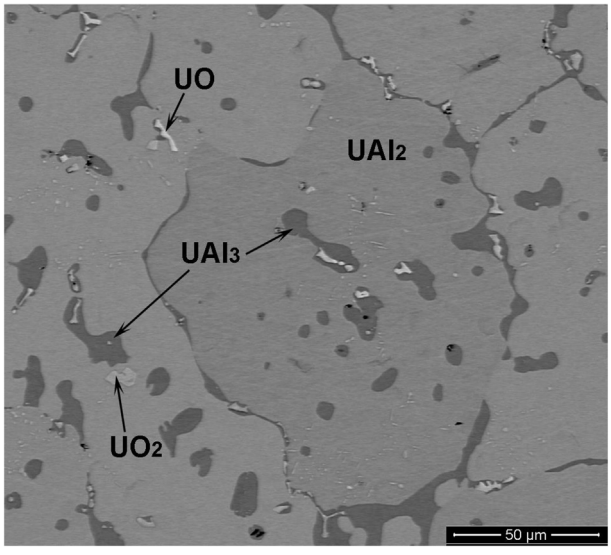

Fig. 2. SEM image of primary UAl_2 ingot (backscattered electrons). Four phases can be seen.

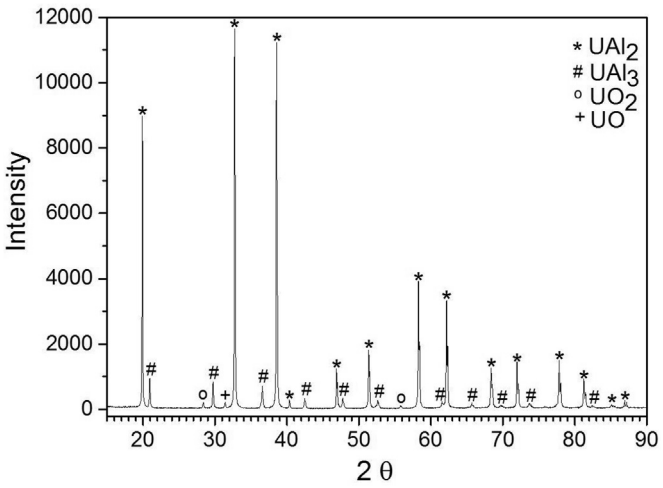

Fig. 3. X-ray diffraction revealing the presence of the UAl_2, UAl_3, UO_2 and UO phases in the UAl_2 whose microstructure is shown in Fig. 2.

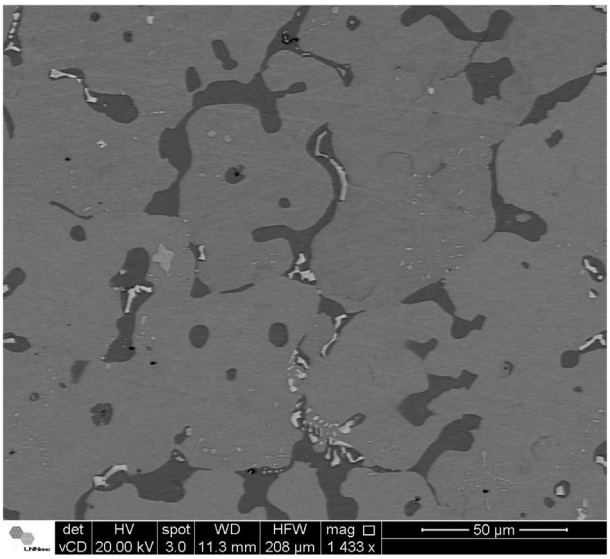

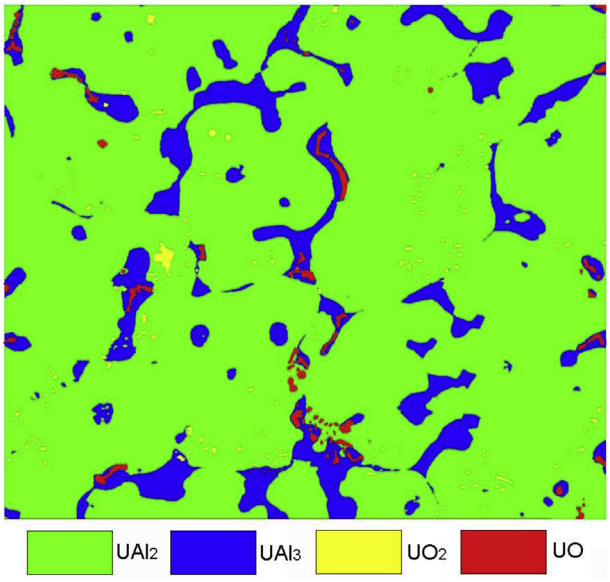

Fig. 4. Example of phase discrimination for area fraction quantification in the UAl_2 ingot.

phase, with UAl_3 being the minority phase. From a practical point of view, it is difficult to produce any alloy in a single phase. A small but finite quantity of phases at the left or at the right sides of the target compound in the phase diagram is expected to be found. This deviation from the exact stoichiometry is due to the inevitable oxidation and/or evaporation of the alloying elements during melting, and has been reported in the literature for the U-Si system [33] and also for the U-Al [5] system.

The presence of oxides in UAl_2 has been reported by Ali et al. [5] that detected the presence of oxides in concentrations between 2 and 4.7 wt% in their UAl_2 samples synthetized by arc melting. These authors did not discriminate the composition of the oxides and they identified them as UO/UO_2. Kohut et al. [9] observed UO_2 peaks in the diffractogram from their UAl_2 samples made by induction melting. The presence of these oxides is difficult to avoid due to the high reactivity of the uranium metal used as raw material. Small amounts of oxygen present as a contaminant in the furnace atmosphere cause oxidation. In this work, an induction furnace was used, and it was possible to see an oxide layer growing over the molten metal during the melting. The oxide layer grows to a critical thickness which breaks due to the turbulence of the molten metal generated by the induction and is incorporated into it.

Regarding phase quantification by image analysis, backscattered electron images were collected from polished UAl_2 samples and analyzed. A total of seven images were analyzed and the area fraction of each phase was determined. From stereology, it follows that the area fraction is equivalent to volume fraction. As a result, the mass fraction of each phase could be calculated. The densities used in mass fractions calculations were 8.26 g/cm^3 for UAl_2 [25], 6.83 g/cm^3 for UAl_3 [26], 10.96 g/cm^3 for UO_2 [28] and 14.16 g/cm^3 for UO [29].

The image analysis software discriminates each phase based on its gray levels and determines the area fraction of each level. The magnification used was 1400× and image resolution was 0.2 µm/pixel. The determination of the gray level range for each phase was performed manually. One of the images (sample 1) was analyzed by three different operators to evaluate the between-operators variation. In Fig. 4 is shown an example of phase discrimination for area fraction quantification and the results obtained from each measurement are presented in Table 3. The example shown in Fig. 4 refers to Sample 3 of Table 3.

Table 3
UAl_2 phase quantification by image analysis in the ingot.

sample	phase							
	UAl_2		UAl_3		UO_2		UO	
	vol%	wt%	vol%	wt%	vol%	wt%	vol%	wt%
1/operator1	86.8	88.2	12.3	10.3	0.4	0.6	0.5	0.9
1/operator2	86.9	88.4	12.2	10.2	0.5	0.7	0.4	0.7
1/operator3	87.2	88.5	11.8	9.9	0.3	0.4	0.7	1.2
mean		88.4		10.1		0.6		0.9
st. dev.		0.2		0.2		0.2		0.3
2	85.7	87.0	12.9	10.8	0.6	0.8	0.8	1.4
3	86.9	87.5	11.0	9.2	0.8	1.1	1.3	2.2
4	87.9	89.7	9.9	8.4	0.4	0.5	0.8	1.4
5	86.8	87.8	11.6	9.7	0.7	0.9	0.9	1.6
6	90.0	90.9	9.0	7.6	0.4	0.5	0.6	1.0
7	85.4	86.5	12.8	10.7	0.8	1.1	1.0	1.7
mean		88.3		9.5		0.8		1.5
st. dev.		1.6		1.2		0.3		0.4

The results showed a small variation between operators in phase quantification by image analysis. Considering UAl_2 and UAl_3 the uncertainties from the measurements performed by different operators were significantly lower than those results from the measurements of all samples, including the mean obtained in sample 1. For the case of the oxide inclusions, the variability regarding operators was slightly larger. This occurred probably due to the difficulty of discriminating these phases in image processing, which increases the uncertainty.

Chemical analysis determined the uranium content as 80.74 wt %, with a uranium loss of 0.76 wt% compared to nominal uranium content of the initial charge composition (81.50 wt% U). This loss was attributed to uranium oxidation during the heating and melting process. As a result, the alloy became hypostoichiometric and UAl_3 was formed, as observed by electron micrograph (Figs. 2 and 4).

Taking into account the uranium content determined by chemical analysis and neglecting the presence of oxide phases remaining in the sample for the calculation, the expected phase composition would be about 89.0 wt% UAl_2 and 11.0 wt% UAl_3. These values are close to the values shown in Table 3, giving an indication of the accuracy of the image analysis method.

The density measured for the powder was 8.13 g/cm^3. Assuming the theoretical density of UAl_2 is 8.26 g/cm^3 [25], the theoretical density of UAl_3 is 6.83 g/cm^3 [26] and neglecting the presence of oxide phases for the calculation, the expected phase composition would be about 90.9 wt% UAl_2 and 9.1 wt% UAl_3. These values are also in agreement with those obtained by the image analysis method. They are higher than the calculated compositions because of the presence of high density oxides.

Another possibility for phase quantification in the primary UAl_2 compound is X-ray diffraction. In their work, Ali et al. [5] quantified the phases present in UAl_2 using X-ray diffraction. The quantification was carried out by comparing the highest peak intensities of each phase, i. e. crystal plane (2 2 0) for UAl_2, crystal plane (1 1 1) for UAl_3 and crystal plane (1 1 1) for UO. In their work, Ali et al. [5] did not quantify the oxide phases UO_2 and UO separately, presenting results for both UO/UO_2 phases. The UO_2 peaks were not observed in the diffractogram presented in their work.

In the present work, X-ray diffraction with the Rietveld method [31,32] was applied to phase quantification. The results were then compared with those obtained by image analysis.

The quality evaluation of a Rietveld refinement depends on the assessments that are made in several calculated parameters in the simulation, such as the difference between the experimental and simulated diffractograms (shown in Fig. 5), the calculated cell parameters, the calculated density for the structures, and R-factors. The x-ray diffraction pattern of the UAl_2 powder as well as the phase refinement for identification and quantification of their fractions are shown in Fig. 5.

The result of phase quantification by X-ray diffraction is shown in Table 4, along with the result obtained by image analysis. The uncertainty presented for the result obtained by the X-ray diffraction method is that provided directly from the TOPAS program used for the refinement. The uncertainty presented for the result from image analysis method was obtained from the mean of seven measurements.

The data presented in Table 4 show consistent results for phase quantification by both methods allowing them to be applied for phase quantification in the primary UAl_2 ingot. The lower value of the UO_2 concentration obtained by the image analysis method can be attributed to the difficulty of its discrimination, being confused with the UAl_2. The uncertainties associated with the quantification of phases by the X-ray diffraction method will be discussed later in Section 3.5.

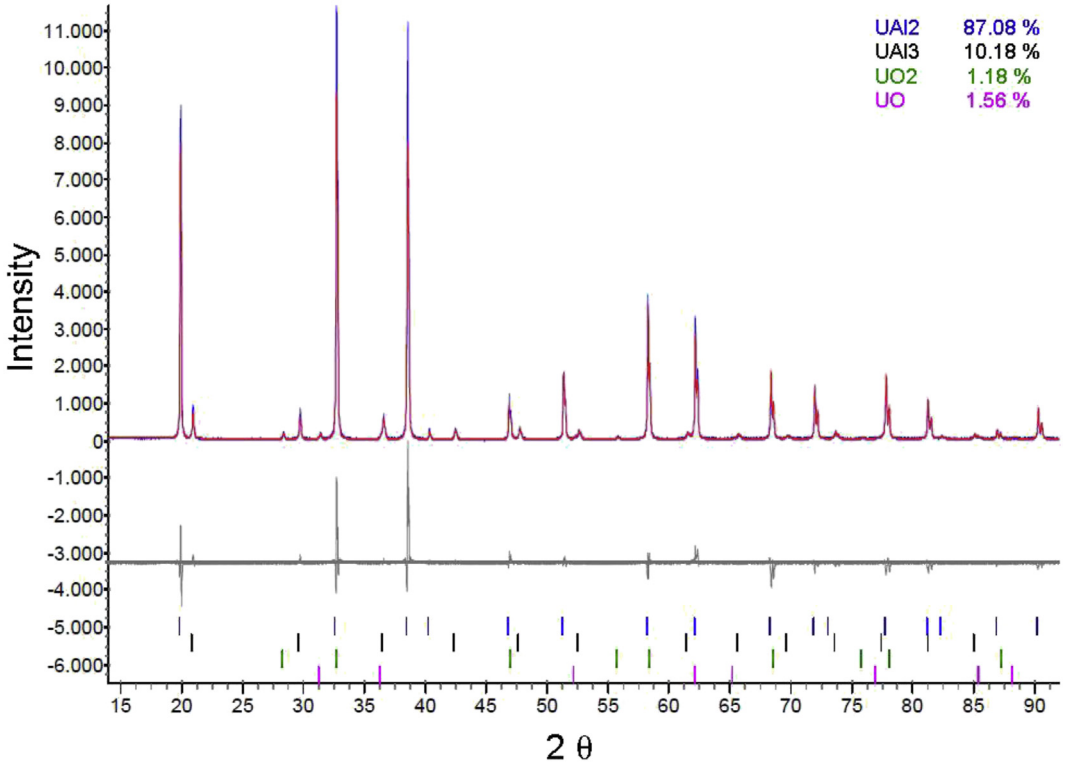

Fig. 5. X-ray diffraction powder pattern of the UAl_2 with Rietveld refinement.

Table 4
Compared results of phase quantification in UAl_2.

phase	image analysis (wt%)	X-ray diffraction (wt%)
UAl_2	88.3 ± 1.6	87.1 ± 0.3
UAl_3	9.5 ± 1.2	10.2 ± 0.3
UO_2	0.8 ± 0.3	1.2 ± 0.1
UO	1.5 ± 0.4	1.6 ± 0.1

3.2. Phase quantification in UAl_x–Al dispersions

Both methods were also applied to phase quantification in UAl_x-Al dispersions. The main application of the methods was to follow the reactions between the aluminides and the aluminum matrix during target fabrication in order to develop a thermo-mechanical treatment aiming at the elimination of the UAl_2 phase. Another application was to quantify the uranium aluminide contents in the finished target.

A typical scanning electron micrograph of a UAl_x-Al briquette is shown in Fig. 6, where the UAl_x particles are homogeneously dispersed in the aluminum matrix. Because of the atomic number contrast from the backscattered electrons, which is sensitive to the composition, it was possible to observe the aluminum matrix of the dispersion (in black) and the shades of gray which refer to the aluminide phases present in the dispersion. The phases were quantified by image analysis using seven images and the results are presented in Table 5. A magnification of 100× was used to give a representative image of the dispersion. An example of phase discrimination to quantify the area fraction is shown in Fig. 7. The image resolution was 1.7 μm/pixel and the density used to calculate the aluminum mass fraction was 2.70 g/cm^3 [30].

Table 5 shows that the volume fraction of the aluminum matrix plus the volume fraction of pores presented a mean value of 54 vol %, in agreement with the nominal value of the dispersion, 55 vol%. The discrimination of pores is not possible in the image obtained by scanning electron microscopy with backscattered electrons. For this reason, the weight fraction was overestimated with respect to the added fraction of 27.4 wt%.

The data in Table 5 were normalized to the uranium aluminides phases and are presented in Table 6. These results show highly overestimated values for the UAl_3 concentrations, much higher than the concentration present in the original UAl_2 ingot (see Table 4). This overestimation occurs due to the image generated by the UAl_x-Al dispersion, in which the edges of the UAl_2 particles appear in a darker gray shade and are misinterpreted by the software as being the UAl_3 phase. This can be seen in Fig. 7. As a result, the UAl_3 phase in the dispersion is overestimated. This misinterpretation can be best seen in Fig. 8 where the edges of the UAl_2 particle (lighter gray) are shown shaded and are misinterpreted as being the UAl_3 phase (darker gray) and aluminum from the matrix (black).

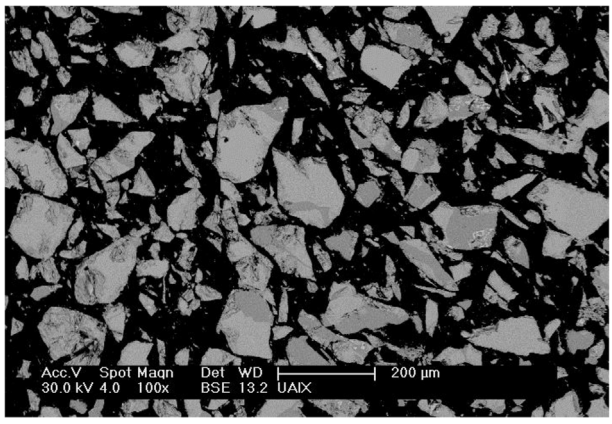

Fig. 6. Scanning electron micrograph from the UAl_x-Al briquette illustrating the dispersion and the phases present (backscattered electrons).

Another limitation of the image analysis method for phase quantification in the UAl_x-Al dispersion was the difficulty of discriminating the UO_2 phase, owing to the low magnification that must be used to obtain representative image of the dispersion. The UO_2 phase is very small (less than 10 μm) with a shade of gray very close to UAl_2.

These limitations make the image analysis method unsuitable to quantify phases in the dispersion.

The X-ray diffraction method was also applied to quantify phases in the UAl_x-Al dispersion. A polished sample of the dispersion was analyzed, and the Rietveld method was used to refine the data. The first result showed an overestimated value for the aluminum concentration when compared to the nominal concentration (27.4 wt%). This was attributed to the effect of microabsorption [34].

The UAl_x-Al dispersion has a low atomic number element (Al) that was mixed with a compound with a high atomic number (U). This situation makes the X-ray interaction with the sample undergo a significant change. UAl_2 has a very high linear absorption coefficient (μ), around 2100 cm^{-1}, when compared to Al which has a coefficient of 130 cm^{-1}. This difference implies that one part of the UAl_x particle can "shadow" the rest of its own grain. If the particle size is comparable to the absorption length 1/μ of the compound, the portion of the particle that is being irradiated will suppress the diffraction potential of the grain volume. For instance, the 1/μ for UAl_2 is 4.7 μm of x-ray penetration in the material, contrasted with 77 μm in Al. This phenomenon is known as microabsorption [34] and is caused by heterogeneity of absorptions at the granular level (in the particle). One of the consequences that can occur in this phenomenon is the overestimation of the intensity of the compound of low absorption, although it is difficult to predict all the effects caused.

In the mid-1940s Brindley [34] developed a correction that can be incorporated into the Rietveld refinement in order to correct or minimize the microabsorption effect. This correction takes the difference between the linear absorption coefficients of the phase being analyzed and the sample itself into account, additionally it considers the mean particle size of the sample in question. In this way, the correction was applied to the refinement and Table 7 shows the results obtained with and without Brindley's correction. Table 8 shows the data normalized to the uranium aluminide phases.

With the application of Brindley's correction, the value of the aluminum concentration in the dispersion was close to the nominal concentration (27.4 wt%) giving a variation around 2%. Brindley's correction also increased by 6.5% the UAl_2 concentration. It is worth pointing out that as the UAl_2 content was higher with corrections and if eliminated from the target, using Brindley's correction provides assurance that all UAl_2 will be consumed during the target fabrication. Additionally, the aluminum concentration in the dispersion became compatible with the nominal value. Therefore the Brindley correction was applied in the phase quantification of the UAl_x-Al dispersion.

3.3. Application of the method for adjusting the thermo-mechanical process

The applicability of the X-ray diffraction method for UAl_x phase quantification was tested on targets fabricated by hot-rolling at

Table 5
Results of phase quantification in the UAl_x-Al dispersion by image analysis.

sample	phase									
	UAl_2		UAl_3		UO_2		UO		Al	
	vol%	wt%	vol%	wt%	vol%	wt%	vol%	wt%	vol%	wt%
1	22.9	38.0	23.8	32.6	nd	nd	0.2	0.6	53.1	28.8
2	19.7	33.0	26.1	36.2	nd	nd	0.5	1.4	53.7	29.4
3	18.5	31.5	26.8	37.8	nd	nd	0.1	0.3	54.6	30.4
4	21.2	36.1	23.1	32.6	nd	nd	0.1	0.3	55.6	31.0
5	19.3	32.0	28.2	38.6	nd	nd	0.4	1.1	52.1	28.2
6	21.8	36.4	24.5	33.8	nd	nd	0.2	0.6	53.5	29.2
7	19.7	33.6	24.8	35.0	nd	nd	0.2	0.6	55.3	30.8
mean	20.4	34.4	25.3	35.2			0.2	0.7	54.0	29.7
st. dev.	1.6	2.5	1.8	2.4			0.2	0.4	1.2	1.1

nd = not detected.

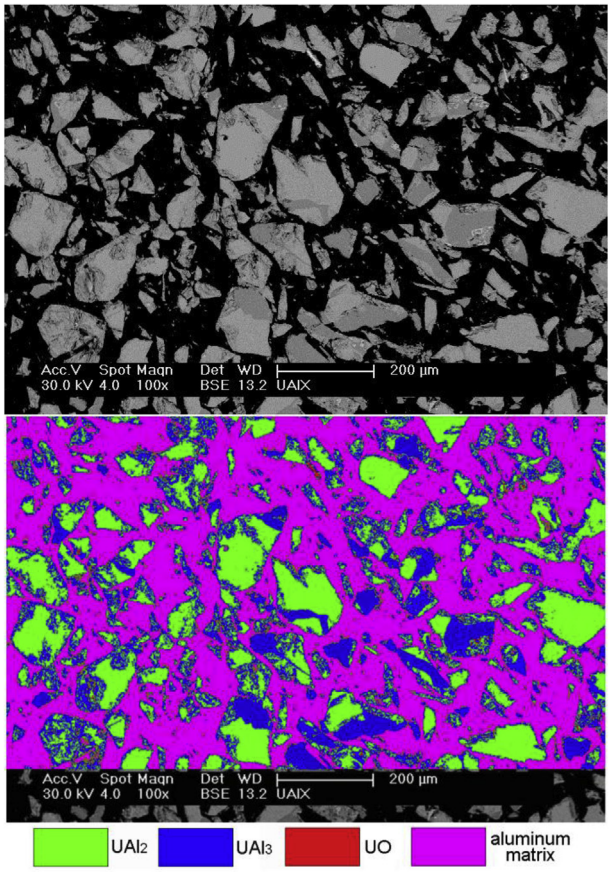

Fig. 7. Example of phase discrimination for area fraction quantification in the UAl_x-Al dispersion.

different temperatures. After hot-rolling, the targets were annealed at the rolling temperature and were removed after different cumulative times for phase quantification. The final heat treatment was performed to evaluate the evolution of the UAl_x phases over time. The objective was to consume all of the UAl_2 phase.

The rolling temperatures studied were 440 °C, which is the usual temperature used in the routine manufacture of fuel plates; 540 °C, which is the maximum temperature technologically possible (due to the end defects [17]), and 480 °C, which was adopted as an intermediate temperature.

The evolution of the UAl_x phases during the heat treatment is shown in Fig. 9. The UAl_2 consumption rate enhances significantly when the temperature increases, as can be observed in Fig. 10. At

Table 6
Results from Table 5 normalized to the uranium aluminides phases.

sample	phases			
	UAl_2	UAl_3	UO_2	UO
	wt%	wt%	wt%	wt%
1	53.4	45.8	nd	0.8
2	46.7	51.3	nd	2.0
3	45.3	54.3	nd	0.4
4	52.3	47.2	nd	0.4
5	44.6	53.8	nd	1.5
6	51.4	47.7	nd	0.8
7	48.6	50.6	nd	0.9
mean	48.9	50.1		1.0
st. dev.	3.5	3.3		0.6

the usual manufacturing temperature, i.e. 440 °C, the UAl_2 concentration remained high (above 10 wt%) even after 18 h of heat treatment. At 480 °C, UAl_2 was virtually eliminated after 14 h of heat treatment. At 540 °C, elimination of UAl_2 occurred after 7 h of heat treatment. UAl_4 formation, due to the reaction between UAl_3 and aluminum matrix, increases significantly after 5 h of heat treatment at 540 °C, slightly after 10 h at 480 °C, and is practically not formed at 440 °C even after 18 h of heat treatment. The predominant phase after 7 h at 540 °C is UAl_4.

The oxide concentration (UO plus UO_2) remained practically constant at the level as in the original powder of around 1.5 wt% (Table 8). The plot hot-rolling at 480 °C shows points in triplicate originated by three different targets. This was done to evaluate the reproducibility of the heat treatment, as will be discussed.

From the data presented above it can be concluded that 7 h' heat treatment at 540 °C is sufficient to consume all of the UAl_2 initially present in the target. The value found for the UAl_2 concentration after 7 h of heat treatment at 540 °C was 0.2 ± 0.1 wt%. The heat treatment time was increased to 9 h to verify if this UAl_2 residue could be further decreased. The result after 9 h was found to be 0.7 ± 0.2 wt%. This observation shows that the X-ray diffraction method is not sensitive to such low concentrations of UAl_2. This indicates that these values should be neglected and assumed to be zero.

A detailed examination of the experimental diffractograms did not indicate the presence of reflections for the UAl_2. It was not possible to observe any perturbation in the background of the diffractograms at the positions 2θ referring to the characteristic reflections of UAl_2. The reflections examined were (1 1 1) at position 2θ of 19.77° with 77.9% relative intensity, and (2 2 0) at position 2θ of 32.56° with 100% relative intensity. The third more intense reflection (3 1 1) for UAl_2 is coincident with the (1 1 1) reflection of aluminum and could not be examined. Fig. 11A is shows the

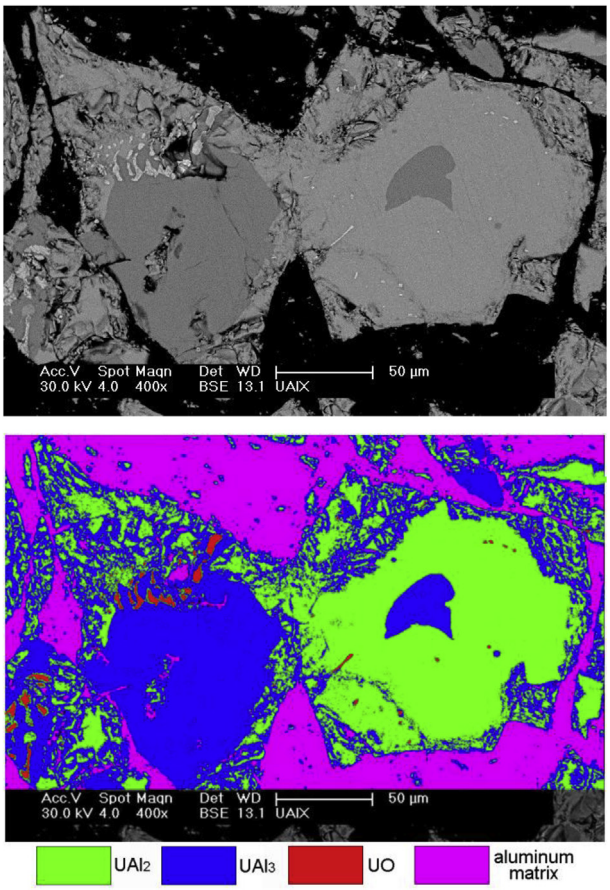

Fig. 8. Example of overestimation of UAl_3 due to shading of edges of UAl_2 particles.

Table 7
Results of phase quantification in the UAl_x-Al dispersion by X-ray diffraction.

phase	without correction (wt%)	with correction [34] (wt%)
Al	58.4 ± 0.5	26.8 ± 0.4
UAl_2	36.3 ± 0.4	68.1 ± 0.5
UAl_3	4.3 ± 0.2	4.1 ± 0.3
UO_2	0.4 ± 0.1	0.4 ± 0.1
UO	0.6 ± 0.1	0.6 ± 0.1

Table 8
Results from Table 7 normalized to the uranium aluminides phases.

phase	without correction (wt%)	with correction [34] (wt%)
UAl_2	87.3 ± 1.4	93.0 ± 0.9
UAl_3	10.3 ± 0.5	5.6 ± 0.4
UO_2	1.0 ± 0.2	0.5 ± 0.1
UO	1.4 ± 0.2	0.8 ± 0.2

diffractogram obtained from the sample treated at 540 °C for 7 h and in Fig. 11B is shown details of the background of the diffractogram evidencing the absence of the reflections (1 1 1) and (2 2 0) for UAl_2 (region indicated on Fig. 11A). Based on these observations, it was concluded that the heat treatment at 540 °C for 7 h consumed all existing UAl_2 in the UAl_x-Al dispersion.

The transformation of UAl_2 to UAl_3/UAl_4 results in a considerable increase in volume due to the lower densities of aluminum rich aluminides. The density of UAl_2 is 8.26 g/cm^3 [25], that of UAl_3 is 6.83 g/cm^3 [26], and that of UAl_4 is 6.08 g/cm^3 [27]. The high volume increase was observed in the samples after heat treatment at

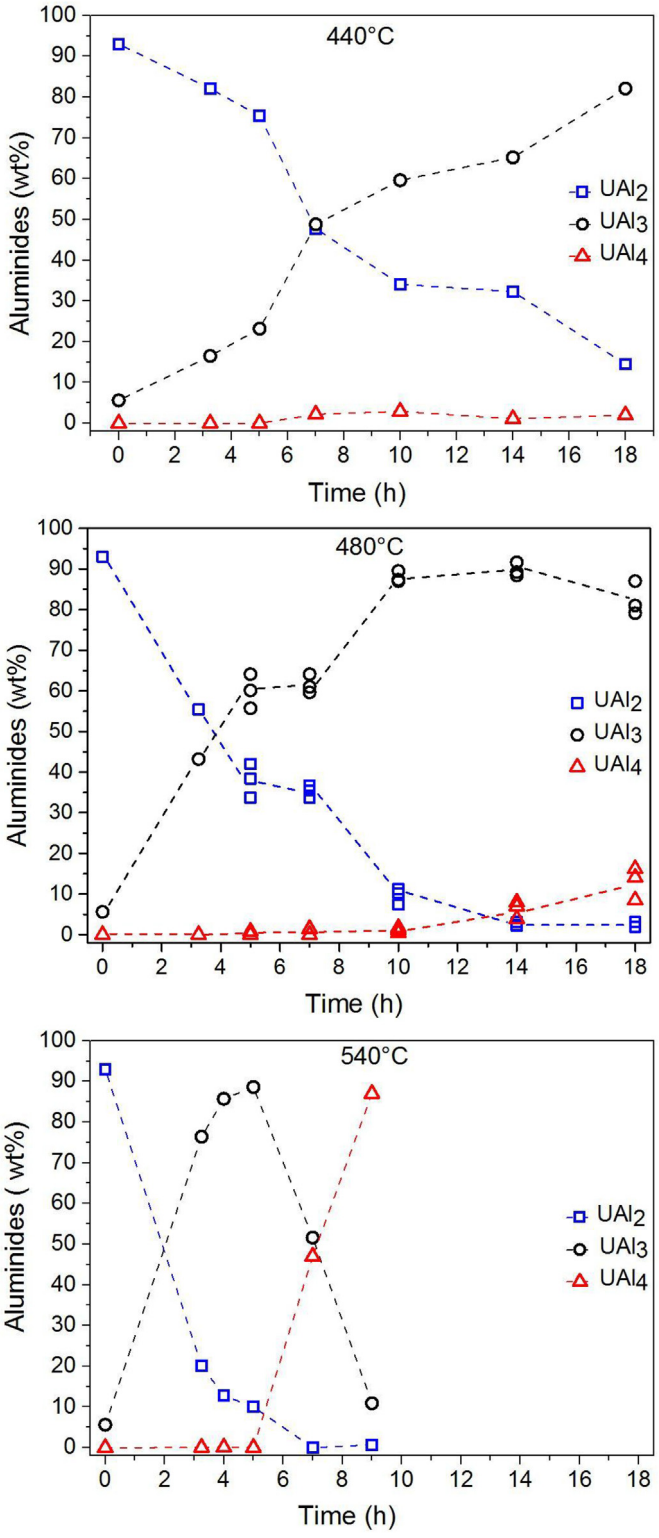

Fig. 9. Evolution of the UAl_x phases during the heat treatment at different temperatures.

540 °C for 9 h, as shown in Fig. 12. Assuming the composition of 10 wt% UAl_3 and 90 wt% UAl_4 after the heat treatment (see Fig. 9) the volume increase was estimated to be around 25%.

This exaggerated swelling is undesirable in cold-rolling, which can cause damage to the surface of the target at the end of the meat

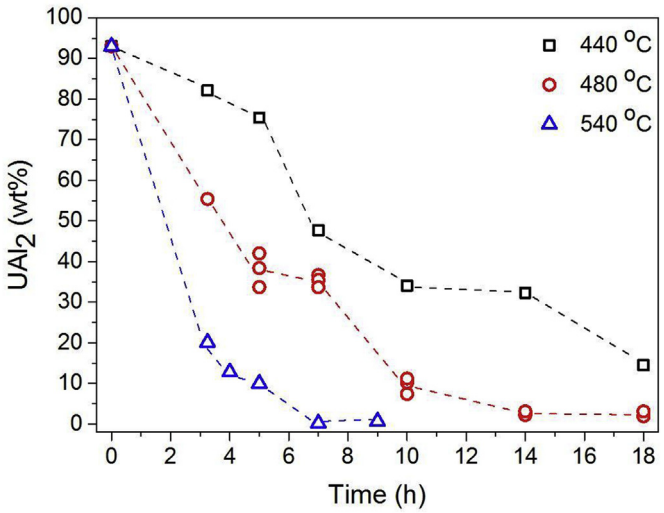

Fig. 10. Effect of temperature on UAl_2 consumption.

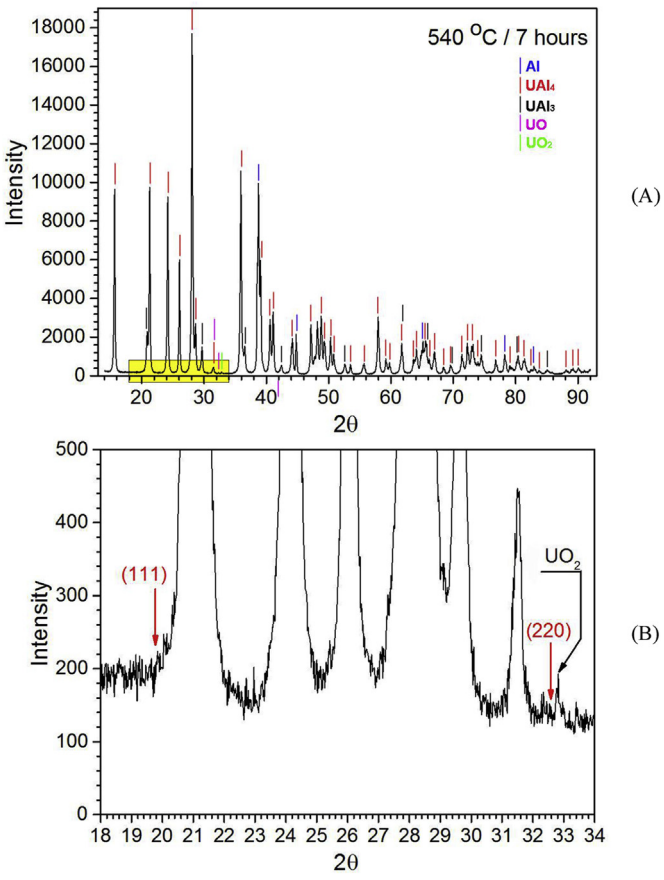

Fig. 11. (A) Diffractogram evidencing the absence of the UAl_2 phase after 7 h of heat treatment at 540 °C. (B) Details of the background indicated in (A).

such as cracks and marks, as well as problems of dog-boning and fish-tail end defects [17]. For this reason, the UAl_2 transformation in UAl_3 and UAl_4 should be distributed along the hot-rolling process so that part of the volume increase due to the reaction is gradually absorbed during the hot-rolling. This new manufacturing procedure was then tested.

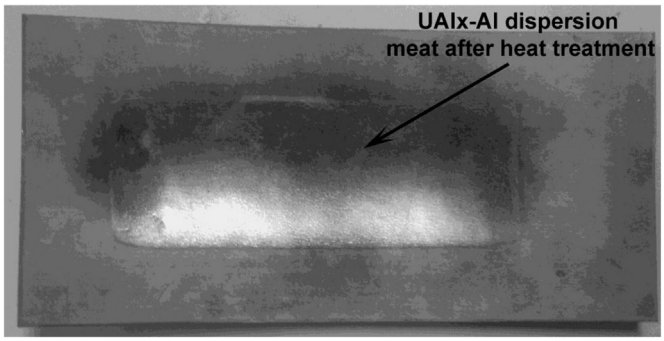

Fig. 12. Increase of target meat due to transformation of UAl_2 into UAl_3 and UAl_4 (after heat treatment at 540 °C for 9 h).

3.4. Application of the method in a real manufacturing test

The heating time between hot-rolling passes was adjusted to better distribute the UAl_2 transformations to UAl_3 and UAl_4. The fabrication test was performed by hot-rolling the targets at 540 °C with re-heating for 36 min between passes. Before the first hot-rolling pass the assemblies were heat treated for 1 h at 540 °C. After each hot-rolling pass, a target was withdrawn for phase quantification. After hot-rolling, seven samples were analyzed for aluminide phases after heat-treatment for 3 h. Table 9 shows the sampling scheme to evaluate the UAl_x phase composition during the rolling and after the final heating treatment necessary to consume all UAl_2 phase. The total time at 540 °C was 420 min (7 h).

Fig. 13 shows the profile evolution of the aluminide content in the target meat during the manufacturing. In pass 2 of hot-rolling (96 min at 540 °C) the formation of UAl_3 was already evident. In pass 5 of hot-rolling (204 min at 540 °C) the maximum concentration of UAl_3 was observed. It was also noted that a substantial decrease of UAl_2 was observed, which included the beginning of the UAl_4 formation. At the end of the manufacture process (pass 6—240 min at 540 °C) the concentration of UAl_2 was already very small and the consumption of UAl_3 became more pronounced, forming UAl_4. Based on the background inspection of the diffractogram, where the reflections (1 1 1) and (2 2 0) were not observed, it can be stated that after 7 h of accumulated heat treatment the UAl_2 was no longer present. At the end of manufacture, the concentration of UAl_4 was preponderant.

By producing targets according to this procedure, it was possible to carry out cold-rolling without the observation of terminal defects. Dog-boning could be suitably controlled.

Comparing the evolution of the UAl_x phases in the manufacturing test (Fig. 13) with the data presented in Figs. 9 and 10, it can be observed that UAl_2 consumption was much faster in the manufacturing test than in the heat treatment at 540 °C after rolling. After 4 h at 540 °C, the UAl_2 concentration in the manufacturing test (virtually zero) was much lower compared to the concentration after 4 h heat treatment after rolling (about 12 wt %). In addition, after that time, the formation of UAl_4 was already advanced. This behavior could be explained by the fragmentation of UAl_2 particles during rolling. Due to the fragmentation, new areas of UAl_2 particles are exposed favoring the reaction with the aluminum matrix, forming UAl_3. The increase of the heating time between hot-rolling passes possibly increased the amount of UAl_2 reacted after each pass, in a cumulative effect. In the subsequent pass, new unreacted free surface of UAl_2 particles will be reacted in greater quantity, which accelerates the reaction with aluminum matrix. This is evidenced in the electron micrographs shown in Fig. 14. The reaction around cracks in the UAl_2 particles can be

Table 9
Sampling scheme for following the UAl_x phase evolution during target fabrication.2

target number		thickness of picture-frame assembly (mm)					
		P1	P2	P3	P4	P5	P6
1	heat → withdrawn for analysis (WA) after 1 h at 540 °C						
2		7.04 → WA					
3		7.09	5.21 → WA				
4		7.06	5.19	3.96 → WA			
5		7.10	5.20	3.90	2.80 → WA		
6		7.05	5.22	3.98	2.85	2.21 → WA	
7		7.05	5.21	3.95	2.83	2.28	1.70 → WA
8	heat → withdrawn for analysis (WA) after 3 h at 540 °C						

P 1 – 6 : hot-rolling pass WA : withdrawn for phase quantification

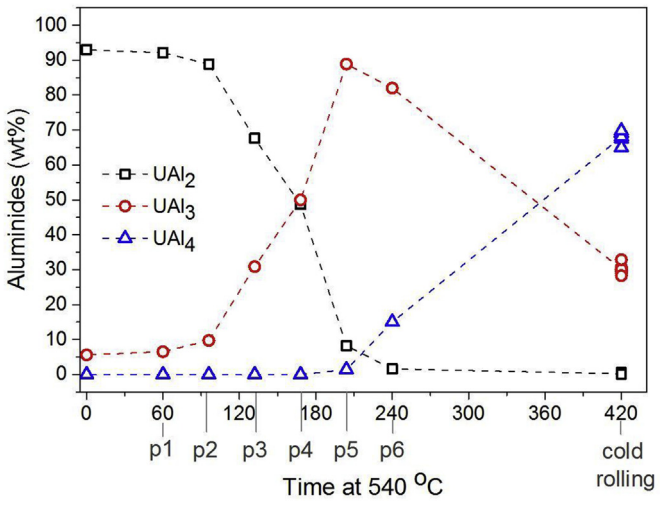

Fig. 13. Evolution of aluminides during true fabrication of target.

observed. Small UAl_2 fragments are virtually transformed into UAl_3 while the interior of the larger particles have not yet been transformed. The image was obtained after heat treatment which followed the second hot-rolling pass (pass p2, Fig. 13) with accumulated time of 132 min thermal treatment.

The dispersion of the results after fabrication is shown in Fig. 13 for seven samples taken from three fabricated targets. Most of the dispersion can be explained by the UAl_2 particles fragmentation, which should not be perfectly reproducible during rolling. A discussion about the precision and accuracy of the method for phase quantification is presented in the following.

3.5. Considerations about precision and accuracy of the method

The Rietveld method is nowadays the most employed methodology to achieve quantitative phase analysis of crystalline materials in general [35,36]. The issue of precision and accuracy in quantitative phase analysis via X-ray diffraction is a difficult one. This topic has been discussed since 1979 in the Accuracy in Powder Diffraction Conferences, which are held approximately every ten years at National Institute of Standards and Technology - NIST. Many factors can affect precision and accuracy [36,37]. Determining uncertainties in a non-standard method, such as the Rietveld method, is not a simple matter. Citing uncertainties based only on the mathematical precision of the fit model to the observed data is not appropriate since they should be underestimated [36].

Methods to calculate uncertainties in quantitative phase analysis are generally not presented in publications. Normally, only uncertainties calculated by the Rietveld-based software are presented. The results are often quoted as Rietveld wt% ± Rietveld uncertainty, as those in the present work presented in Tables 4 and

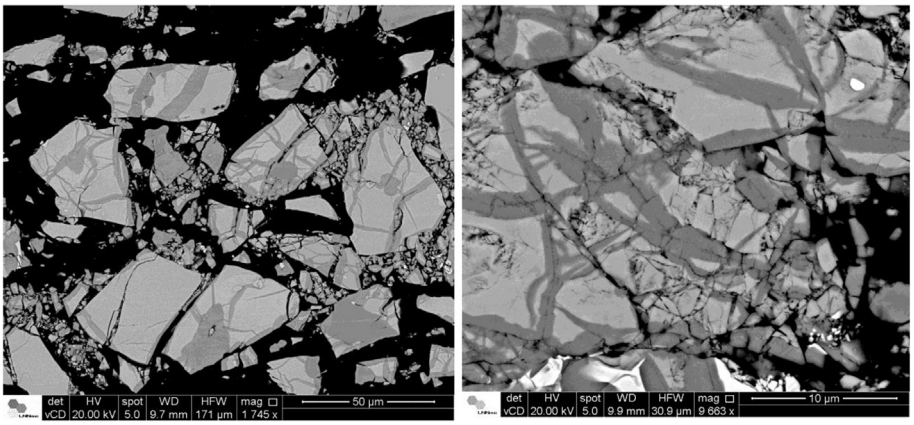

Fig. 14. Evidence of the UAl_2 particle fragmentation favoring its reaction with the aluminum matrix to form UAl_3 (light gray = UAl_2, dark gray = UAl_3).

7 However, refinement uncertainties by Rietveld indicate just how the model is adjusting the observed diffraction pattern. The determination of real precision is not simple. Even analyzing replicates, the uncertainty may be underestimated.

To evaluate accuracy it would be advisable to use a standard with known concentrations of the phases. The error will only be determined if the concentrations are already known. In the case of the present work, we are confronted with the problem of preparing pure phases in practice.

The main errors for quantitative phase analysis are preferred orientation, amorphous content and microabsorption. The problem of microabsorption appears to be the biggest physical hindrance to accurate quantitative phase analysis using X-ray diffraction data. The most commonly used correction method for microabsorption was that of Brindley [34] in conjunction with Rietveld pattern analysis methods. A slight improvement in results was achieved when the Brindley method was applied, but it would appear that, in this instance, the severity of the problem was beyond the limits of the correction algorithm [36]. The Brindley method is most successful when combined with sample preparation strategies that minimized the problem prior to data collection. One of the most basic sources of error is the failure to grind samples. Unfortunately, this was impossible in the present work because of its purpose, in which the dispersion cannot be modified.

As an example, Scarlett and Madsen [38] analyzed a known mixture of Al_2O_3, Fe_3O_4 and $ZrSiO_4$. The Rietveld uncertainty (around ± 0.15 wt%) quadrupled when samples in triplicate were analyzed. In addition, replication uncertainties only indicate the precision of the measurement. In the same sample, which had a known composition, the concentration values varied up to 6 wt% from the nominal value. Therefore, accuracy is an important issue.

In the present work, the question of accuracy is very difficult to evaluate due to the challenge of preparing pure aluminide standards, as already mentioned. However, in the case of the UAl_2 primary ingot, the comparison of the results obtained between X-ray diffraction and image analysis methods shows coherence and approaches the values calculated from the values derived from the uranium chemical analysis and density, as shown in Table 10. Remember that the calculated values from analysis neglected the presence of the oxides, which causes an impact on accuracy. In the case of UAl_x-Al dispersions, the image analysis method cannot be applied due to the error already discussed which causes an unacceptable deleterious effect on accuracy.

To evaluate the precision of the X-ray diffraction method applied to UAl_x-Al dispersions, samples were analyzed in triplicate. To do that, three diffractograms were obtained from a single sample of a target fabricated at 540 °C heat-treated for 7 h (end of the process). The phases were quantified by the X-ray diffraction method. In addition, two other different samples were taken from this target in two different regions of the meat to evaluate the variation of phase concentrations in different regions of the target.

Another two different targets were analyzed for phase quantification, which were also fabricated at 540 °C heat-treated for 7 h (end of the process) according to the same procedures. The purpose was to evaluate the variability of aluminide concentrations in the manufacturing process.

All results were incorporated in the curve presented in Fig. 13, which allows better visualization of the total dispersion of the results. Table 11 summarizes such results.

The Rietveld uncertainties presented in Table 11 can be considered small, indicating that the model is adjusting the experimental diffraction patterns well. Table 12 summarizes the results that allow visualization of the uncertainties from the X-ray diffraction method (triplicates), the variability of the UAl_x phase concentrations in the same target and the variability in the manufacturing process as a whole. The Rietveld uncertainties were ignored in the calculations, since they only express the refinement quality. The averages and standard deviations for target 2 considered all the results, including the triplicates. The averages and standard deviations for the process considered all the results, including the triplicates and the 3 regions of target 2. Thus, all the uncertainties were considered in the results referring to the process as a whole.

The results presented in Table 12 show that, in general, the method uncertainty is of the order of three times the Rietveld's uncertainties for the phases that remain after the fabrication of the target (UAl_3 and UAl_4). At the same target (target 2), the concentration variability was shown to be of the same order of magnitude as the method variability. This shows that the evolution of the phases within the targets is reproducible. The variability of the concentrations considering the whole process was approximately double the variability of the method and at the same target. This is expected, since the fabrication of targets incorporates the intrinsic variability characteristic of the manufacturing process.

It can be seen from the data in Table 12 that the values of the concentrations of UO and UO_2 remain constant for all samples, around 1.5 wt% (Table 8, with correction). This is expected since these phases are stable in the manufacturing process and their concentration must necessarily remain the same as originally existed in the UAl_2 powder.

The data in Table 12 also show that the concentrations of UAl_2 are always practically zero. This is expected and necessary, since the purpose of the manufacturing process is to consume all UAl_2 in the finished target.

It is beyond the scope of the present work to carry out a detailed study of the calculation of uncertainties on quantitative phase analysis by X-ray diffraction. However, the calculation of significant uncertainties is an important part of the quantitative phase analysis and, as such, should be considered in future studies. Even with the uncertainties that were discussed, the X-ray diffraction method proved to be applicable in the development of the target manufacturing process, being a very useful tool in the development of the thermo-mechanical treatment for the control of UAl_x phases and elimination of the unwanted UAl_2.

Although the method does not completely zero out the UAl_2 concentration, the small values presented for this phase can be considered zero, as confirmed by careful inspection of the background of the experimental diffractograms. All experimental diffractograms of the samples included in Table 11 were inspected and no diffraction peaks for UAl_2 were detected. Fig. 15 shows the background of the experimental diffractogram obtained from the sample that presented the highest concentration of UAl_2, which was fabricated according the procedure developed in the real manufacturing test (target 1).

Table 10
Accuracy of phase quantification in the UAl_2 ingot by both methods studied.

phase	image analysis (wt%)	X-ray diffraction (wt%)	chemical analysis (wt%)	Density (wt%)
UAl_2	88.3 ± 1.6	87.1 ± 0.3	89.0	90.9
UAl_3	9.5 ± 1.2	10.2 ± 0.3	11.0	9.1

Table 11
Quantification[a] of phases by X-ray diffraction in 3 targets fabricated at 540 °C heat-treated for 7 h (end of process).

target	sample	replica	UAl_2 (wt%)	UAl_3 (wt%)	UAl_4 (wt%)	UO (wt%)	UO_2 (wt%)
1			0.5 ± 0.1	32.9 ± 0.2	65.0 ± 0.2	0.2 ± 0.1	1.4 ± 0.1
		1	0.3 ± 0.1	29.0 ± 0.3	69.2 ± 0.3	0.3 ± 0.1	1.2 ± 0.1
	1	2	0.2 ± 0.1	30.7 ± 0.3	67.5 ± 0.3	0.2 ± 0.1	1.4 ± 0.1
2		3	0.1 ± 0.1	29.6 ± 0.3	69.0 ± 0.3	0.4 ± 0.1	0.9 ± 0.1
	2		0.3 ± 0.2	30.2 ± 0.2	68.1 ± 0.3	0.2 ± 0.3	1.3 ± 0.5
	3		0.3 ± 0.2	30.2 ± 0.2	68.0 ± 0.3	0.2 ± 0.3	1.4 ± 0.5
3			0.1 ± 0.1	28.3 ± 0.2	69.8 ± 0.3	0.3 ± 0.1	1.6 ± 0.1

[a] All data were normalized to the aluminide phases.

Table 12
Summary showing uncertainties related to method, target and process as a whole.[a]

	UAl_2 (wt%)	UAl_3 (wt%)	UAl_4 (wt%)	UO (wt%)	UO_2 (wt%)
method (triplicates)	0.2 ± 0.1	29.8 ± 0.9	68.6 ± 0.9	0.3 ± 0.1	1.2 ± 0.3
target 2 (3 regions)	0.2 ± 0.1	29.9 ± 0.7	68.4 ± 0.7	0.3 ± 0.1	1.2 ± 0.2
process (3 targets)	0.3 ± 0.1	30.1 ± 1.5	68.1 ± 1.6	0.3 ± 0.1	1.3 ± 0.2

[a] All data were normalized to the aluminide phases.

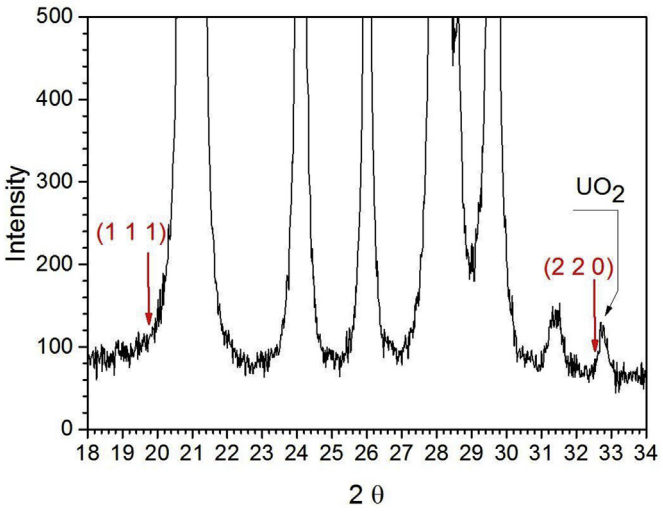

Fig. 15. Detail of diffractogram evidencing the absence of the UAl_2 phase after target fabrication according the procedure developed in this work (target 1/Table 11).

4. Conclusions

The applicability of image analysis and X-ray diffraction methods for phase quantification in UAl_x-Al dispersion targets were studied. The image analysis method showed good results for UAl_x phase quantification in the primary UAl_2 ingot. However, this method presented an unacceptable error when applied to the UAl_x-Al dispersions, which is caused by the difficulty in discriminating the phases in fragmented particles due to the confounding of the gray tones. The lack of accuracy proved to be unacceptable.

The X-ray diffraction method was successfully applied in monitoring the concentrations of the UAl_x phases during the target manufacture. By applying this method, it was possible to develop a suitable thermo-mechanical treatment to consume all UAl_2 phase. The accuracy and precision of this method has been shown to be sufficient for its application for this purpose.

Acknowledgments

The authors are grateful to São Paulo Research Foundation (FAPESP) for the research grant 2011/13849-9 and to CNPq (National Council for Scientific and Technological Development) for the research grant 304034/2015-0 provided for this work. The authors would also like to thank the Brazilian Nanotechnology National Laboratory – LNNano, specifically, Electron Microscopy Laboratory – LME (CNPEM/MCTI) for the technical support with the FEI Inspect F50 to collect images and data.

References

[1] Nuclear Energy Agency, The supply of medical radioisotopes. Organization for economic Co-operation and development (OECD), march 2016. NEA/SEN/HLGMR, 2. (avalaible at: http://www.oecd-nea.org/cen/docs/2016/sen-hlgmr2016-2.pdf, 2016.

[2] J.A. Osso Jr., C.R.B.R. Dias, T.P. Brambilla, R. Teodoro, M.F. Catanoso, J. Zini, R.R.L. Bezerra, L.A. Villela, J.L. Correia, E. Ivanov, F.M.S. Carvalho, L. Pozzo, P.L. Squair, J. Mengatti, Production of 99Mo at ipen-CNEN/SP-Brazil, in: Topical Meeting on Molybdenum-99 Technological Development, Chicago, Illinois, 1–5 April (2013), 2013 (available at: https://mo99.ne.anl.gov/2013/pdfs/Mo99%202013%20Web%20Papers/S9-P1_Osso_Paper.pdf.

[3] I.J. Obadia, J.A. Perrotta, Sustainability analysis of the Brazilian multipurpose reactor project, in: International Topical Meeting Od Research Reactor Fuel Management RRFM 2010, Marrakech, Morocco, 21-25 March, P. 311–315, 2010 (available at: https://www.euronuclear.org/meetings/rrfm2010/transactions/RRFM2010-transactions.pdf.

[4] H.J. Ryu, Y.J. Jeong, J.M. Nam, J.M. Park, Metallurgical considerations for the fabrication of low-enriched uranium dispersion targets with a high density for 99Mo production, J. Radioanal. Nucl. Chem. 305 (2015) 31–39.

[5] K.L. Ali, A.A. Khan, A. Mushtaq, F. Imtiaz, M.A. Zial, A. Gulzar, M. Farooq, N. Hussain, N. Ahmed, S. Pervez, J.H. Zaidi, Development of low enriched uranium target plates by thermo-mechanical processing of UAl_2–Al matrix for production of 99Mo in Pakistan, Nucl. Eng. Des. 255 (2013) 77–85.

[6] H.J. Ryu, C.K. Kim, M.S. Sim, J.M. Park, J.H. Lee, Development of high-density U/Al dispersion plates for Mo-99 production using atomized uranium powder, Nucl. Eng. Technol. 45 (2013) 979–986.

[7] M.S. Sim, H.J. Ryu, J.M. Park, C.K. Kim, J.H. Lee, Dispersion target fabrication for fission Mo using atomized uranium powder, in: Korean Nuclear Society 2013 Spring Meeting. Kyoungju, 29-31 May, 2013, pp. 775–776.

[8] A. Mushtaq, Specifications and qualification of uranium/aluminum alloy plate target for the production of fission molybdenum-99, Nucl. Eng. Des. 241 (2011) 163–167.

[9] C. Kohut, M. Fuente, P. Echenique, D. Podesta, P. Adelfang, Targets development of low enrichment for production of Mo99 for fission, in: Proceeding of International Meeting on Reduced Enrichment for Research and Test Reactors, Las Vegas, Nevada, 1–6 October, 2000 (available at: http://www.rertr.anl.gov/Web2000/Title-Name-Abstract/Fuente00.html.

[10] G.L. Solbrekken, K. Turner, S. Govindarajan, P. Macarewicz, C. Allen, Development, qualification, and manufacturing of LEU-foil targetry for the production of Mo-99, in: International Topical Meeting Od Research Reactor Fuel Management RRFM 2011, Rome, Italy, 20-24 March, P. 233–237, 2011 (available at: http://www.euronuclear.org/meetings/rrfm2011/transactions/RRFM2011-transactions.pdf.

[11] R. Schrader, J. Klein, J. Medel, J. Marín, J. Lisboa, L. Birstein, L. Ahumada, M. Chandía, R. Becerra, X. Errazu, C. Albornoz, G. Silvester, J.C. Jiménez, "Status of the Chilean implementation of the modified Cintichem process for fission

99Mo production using LEU, in: Proceeding of International Meeting on Reduced Enrichment for Research and Test Reactors, Washington, DC, 5–9 October, 2008 (available at: http://www.rertr.anl.gov/RERTR30/index.shtml.
[12] T.C. Wiencek, G.F. Vandergrift, A. Bakel, A.A. Leyva, A.S. Hebden, Status and progress of foil and target fabrication activities for the production of 99Mo from LEU, in: Proceeding of International Meeting on Reduced Enrichment for Research and Test Reactors, Washington, DC, 5–9 October, 2008 (available at: http://www.rertr.anl.gov/RERTR30/index.shtml.
[13] B. Briyatmoko, B. Guswardani, S. Purwanta, S. Permana, D. Basiran, M. Kartaman, Indonesia's current status for conversion of Mo-99 production to LEU fission, in: Proceeding of International Meeting on Reduced Enrichment for Research and Test Reactors, Prague, Czech Republic, 23–27 September, 2007 (available at: http://www.rertr.anl.gov/RERTR29/index.html.
[14] C. Conner, I.E.F. Lewandowsk, J.L. Snelgrove, M.W. Liberatore, D.E. Walker, T.C. Wiencek, D.J. Mcgann, G. l. Hofman, G.F. Vandergrift, Development of annular targets for 99Mo production, in: Proceeding of International Meeting on Reduced Enrichment for Research and Test Reactors, Budapest, Hungary, 3–8 October, 1999 (available at: http://www.rertr.anl.gov/Web1999/Abstracts/Program.html.
[15] J.E. Cunningham, E.J. Boyle, MTR-Type fuel elements, in: International Conference on Peaceful Uses of Atomic Energy, Geneva, 8-20 August, vol. 9, 1955, pp. 203–207.
[16] A.R. Kaufman, Nuclear Reactor Fuel Elements, Metallurgy and Fabrication, Interscience, New York, N.Y, 1962.
[17] M. Durazzo, H.G. Riella, Procedures for Manufacturing Nuclear Research Reactor Fuel Elements, OmniScriptum GmbH & Co. KG, Saarbrücken, Germany, 2015.
[18] B.L. Bramfitt, H.P. Leighly Jr., A metallographic study of solidification and segregation in cast aluminum-uranium alloys, Metallography 1 (2) (1968) 165–193.
[19] H.J. Cols, P.R. Cristini, A.C. Manzini, Mo − 99 from low-enriched uranium, in: Proceeding of International Meeting on Reduced Enrichment for Research and Test Reactors, Las Vegas, Nevada, 1–6 October, 2000 (available at: http://www.rertr.anl.gov/Web2000/Title-Name-Abstract/Cristi00.html.
[20] H. Okamoto, Al-U (Aluminum-Uranium), J. Phase Equilibria Diffusion 33 (6) (2012).
[21] W. Davies, W.Gray, A rapid and specific titrimetric method for the precise determination of uranium using iron(II) sulphate as reductant, Talanta 11 (8) (1964) 1203–1211.
[22] M. Bickel, The Davies-Gray titration for the assay of uranium in nuclear materials: a performance study, J. Nucl. Mater. 246 (1) (1997) 30–36.
[23] C. Motley, "Omnimet Enterprise". Buehler, Lake Bluff, Ill (available at: https://www.dcu.ie/sites/default/files/mechanical_engineering/pdfs/manuals/omniment.pdf, 1998.
[24] Buehler, "Omnimet - solutions for image capture & analysis" Buehler, Lake Bluff, Ill (available at: https://www.lehigh.edu/nano/docs/OmniMet_software.pdf, 2014.
[25] Inorganic Crystal Structure Database. ICSD Collection Code 58195. (available at: https://icsd.fiz-karlsruhe.de/viscalc/jsp/sliderDetailed.action).
[26] Inorganic Crystal Structure Database. ICSD Collection Code 58196. (available at: https://icsd.fiz-karlsruhe.de/viscalc/jsp/sliderDetailed.action).
[27] Inorganic Crystal Structure Database. ICSD Collection Code 240127. (available at: https://icsd.fiz-karlsruhe.de/viscalc/jsp/sliderDetailed.action).
[28] Inorganic Crystal Structure Database. ICSD Collection Code 647597. (available at: https://icsd.fiz-karlsruhe.de/viscalc/jsp/sliderDetailed.action).
[29] Inorganic Crystal Structure Database. ICSD Collection Code 24223. (available at: https://icsd.fiz-karlsruhe.de/viscalc/jsp/sliderDetailed.action).
[30] Inorganic Crystal Structure Database. ICSD Collection Code 43423. (available at: https://icsd.fiz-karlsruhe.de/viscalc/jsp/sliderDetailed.action).
[31] H.M. Rietveld, A profile refinement method for nuclear and magnetic structures, J. Appl. Crystallogr. 2 (2) (1969) 65–71.
[32] R.J. Hill, C.J. Howard, Quantitative phase analysis from neutron diffraction data using the Rietveld method, J. Appl. Crystallogr. 20 (1987) 467–474.
[33] T.C. Wiencek, Summary report on Fuel Development and miniplate Fabrication for the RERTR Program 1978 to 1990, Argonne, Illinois, Argonne National Laboratory, 1995 (ANL/RERTR/TM-15).
[34] G.W. Brindley, The effect of grain or particle size on X-ray reflections from mixed powders and alloys, considered in relaction to the quantitative determination of crystalline substances by X-ray methods, Phil. Mag. 36 (1945) 347–369.
[35] I.C. Madsen, N.V.Y. Scarlett, L.M.D. Cranswick, T. Lwin, Outcomes of the international union of crystallography commission on powder diffraction round robin on quantitative phase analysis: samples 1*a* to 1*h*, J. Appl. Crystallogr. 34 (2001) 409–426.
[36] N.V.Y. Scarlett, I.C. Madsen, L.M.D. Cranswick, T. Lwin, E. Groleau, G. Stephenson, M. Aylmore, N. Agron-Olshina, Outcomes of the international union of crystallography commission on powder diffraction round robin on quantitative phase analysis: samples 2, 3, 4, synthetic bauxite, natural granodiorite and pharmaceuticals, J. Appl. Crystallogr. 35 (2002) 383–400.
[37] J.I. Langford, D.l Louer, Powder diffraction, Rep. Prog. Phys. 59 (1996) 131–234.
[38] N.V.Y. Scarlett, I.C. Madsen, Current state of quantitative phase analysis, in: Accuracy in Powder Diffraction IV Meeting, National Institute of Standards and Technology NIST, Gaithersburg, Maryland, 2013. April 22–23 April.